Subhorizon linear Nash perturbations with joint analysis of cosmic growth and expansion with constrains on $H(z)$ and the deceleration parameter $q(z)$

Abraão J. S. Capistrano* and Hemerson R. Duarte†
Federal University of Latin-American Integration, 85867-670, Foz do Iguassu-PR, Brazil.

Paola T. Z. Seidel‡
PPGCosmo, CCE, Universidade Federal do Espírito Santo, Av. Fernando Ferrari 514, 29075-910, Vitória-ES, Brazil.

(Dated: June 17, 2020)

The Hubble parameter $H(z)$, as a function of redshift, is modified by the presence of a new term originated from the extrinsic curvature in an embedded space-time. Assuming an asymptotic expansion factor $a \sim 0$ or, equivalently $z \to \infty$, it is obtained a nearly resemblance of the present model (β-model) with quintessence wCDM model with $H(z) \sim H_{wCDM}(z)$ at background level. In conjunction with ΛCDM, we test the models using a pack of recent datasets like that of the "Gold 2018" growth data, the best-fit Planck2018/ΛCDM parameters on the Cosmic Microwave Background (CMB), the Baryon Acoustic Oscillations (BAO) measurements, the Pantheon Supernovae type Ia and the Hubble parameter data with redshift ranging from $0.01 < z < 2.3$. Performing the Akaike Information Criterion (AIC) to ascertain the statistical viability of the model from Jeffreys' scale, we apply a joint likelihood analysis to the data with the Markov Chain Monte Carlo (MCMC) method. We find that the present model is in very good agreement with observations with a close statistical equivalence with the ΛCDM and wCDM cosmologies at 1-σ level. We also show that a mild alleviation of the σ tension between the growth amplitude factor and the matter content (σ_8-Ω_m) of the observations from CMB and Large Scale Structure (LSS) probes. A comparison of the aforementioned full pack of data in MCMC chains is made with the resulting MCMC from Pantheon SNIa+$H(z)$ in order to analyse the sensitivity of the models and how they respond to a cosmography analysis on the evolution of $H(z)$ and the deceleration parameter $q(z)$. In this sense, we find that only the β-model can be unaffected to the variations of the previous datasets due to its several minima in the likelihood (degeneracies) of the related parameters with an overall percentage relative difference only up to 4%.

I. INTRODUCTION

After compelling evidences, the accelerated expansion of the universe is constituting one of the greatest challenges for theoretical physics and cosmology. In the last 20 years, the main proposal for the explanation of the current accelerated regime is the well known dark energy hypothesis, consisting in a sort of a cosmological energy with negative pressure that drives the universe to speed up. In this sense, the simplest model for explanation of the accelerated expansion is the popular ΛCDM model. Even though its success, the main components of this model remain in the lack of a fundamental understanding, since the Cosmological constant Λ and the Cold dark matter (CDM) are problems of their own nature [1–7]. These particular problems motivated the investigation of new possibilities for the explanation of the accelerated phase of the universe.

The overall feeling consists in constraining both cosmological and model parameters to grasp an underlying understanding of the fundamental physics on the acceleration expansion problem, whether such component is a time-independent (the cosmological constant) or possesses a dynamical origin. To this matter, an equation of state turns a fundamental cornerstone to confront a model to observational data. For instance, the related dark energy equation of state (EOS) presents a negative fluid parameter, $w = -1$ [8, 9] and competitive models must comply with that value or mild deviations around it with accordance with the latest indications [9].

One of the alternative routes of investigation is being explored by the possibility that the universe might be embedded in extra dimensions. Most of these models have been Kaluza-Klein or/and string inspired, such as, for instance, the seminal works of the Arkani-Hamed, Dvali and Dimopolous (ADD) model [10], the Randall-sundrum model [11, 12] and the Dvali-Gabadadze-Porrati model (DPG) [13]. In all those models and variants, the embedding of geometries is not properly worked as a theoretical background since it is generally fixed to a boundary and specific conditions are needed to obtain their dynamics. Hence, several authors explored embedding of space-times as a promising mathematical structure for a physical theory with the embedding equations as a fundamental mathematical guide [14–27].

In this paper, we perform the Markov Chain Monte Carlo (MCMC) sample technique as a tool for analysing fit-to-data [28–30] in order to constrain the cosmological parameters. The joint likelihood is performed from the latest data on Cosmic Microwave Background (CMB)

* abecapistrano@gmail.com
† r_hemerson@yahoo.com
‡ paola.seidel@gmail.com

Planck 2018 [9], the largest dataset of Pantheon SNIa [31] with redshift ranging from $0.01 < z < 2.3$, the Hubble parameter as a function of redshift $H(z)$ [32–37] and the "extended Gold 2018" compilation to the Planck 2018 (TT, TE, EE + lowE) within the 68% intervals for the best-fit parameters using the data points of SDSS [38–40], 6dFGS [41], IRAS [42, 43], 2MASS [42, 44], 2dFGRS [45], GAMA [46], BOSS [47], WiggleZ [48], Vipers [49], Fast-Sound [50], BOSS Q [51] and additional points from the 2018 SSSD-IV [52–54]. This large pack of data allows us to investigate the tension on the σ_8-contours revealed by the mismatch of the data inferred from Planck CMB radiation and the Large Scale Structure (LSS) observations considering the concordance ΛCDM model as a background. The σ_8 is the r.m.s amplitude of matter density at a scale of a radius $R \sim 8\text{h.Mpc}^{-1}$ within a enclosed mass of a sphere [55]. To allow a proper comparison, we use another MCMC chain with only the model independent measurements on Pantheon SNIa+$H(z)$. Thus, we analyse the response of the cosmography parameters focused on the Hubble function $H(z)$ and the deceleration parameter $q(z)$ with the additional calculations of the related transition redshift z_t. In this manner, we evaluate the sensitivity of the models in combination of the probes commonly used disjointedly in cosmography analysis but explored in several works [56–63].

The paper is organized as follows: in the second section, we make a brief mathematical review on the theoretical framework and its resulting cosmological model. In the third section, the perturbed equations are presented in a conformal Newtonian frame and the related growth equation. The fourth section presents the outcomes and discussions from the comparison of the present model to the models as ΛCDM, quintessense (wCDM) [64, 65] and Chevallier-Polarski-Linder (CPL) [66, 67]. An analysis on the statistical tension between the models is made by using the Akaike Information Criterion (AIC) [68] from the MCMC method. In the final section, we conclude with our remarks and future prospects.

II. THE EMBEDDED MODEL

The gravitational action functional in the presence of confined matter field on a four-dimensional embedded space with thickness l embedded in a D-dimensional ambient space (bulk) has the form

$$S = -\frac{1}{2\kappa_D^2}\int \sqrt{|\mathcal{G}|}\mathcal{R}d^Dx - \int \sqrt{|\mathcal{G}|}\mathcal{L}_m^* d^Dx \,, \quad (1)$$

where κ_D^2 is the fundamental energy scale on the embedded space, $\mathcal{R}$ denotes de Ricci scalar of the bulk and $\mathcal{L}_m^*$ is the confined matter lagrangian. In this model, the matter energy momentum tensor occupies a finite hypervolume with constant radius l along the extra-dimensions. The variation of Einstein-Hilbert action in Eq.(1) with respect to the bulk metric $\mathcal{G}_{AB}$ leads to the Einstein equations for the bulk

$$\mathcal{R}_{AB} - \frac{1}{2}\mathcal{G}_{AB} = \alpha^\star \mathcal{T}_{AB} \,, \quad (2)$$

where $\alpha^\star$ is energy scale parameter and $\mathcal{T}_{AB}$ is the energy-momentum tensor for the bulk [16, 17, 20]. To generate a thick embedded space-time is important to perturb the related background and it can be done in accordance with the confinement hypothesis of gauge interactions that depends only on the four-dimensionality of the space-time [69, 70] in accordance with current phenomenology [71].

Nash's original embedding theorem [72] used a flat D-dimensional Euclidean space, later generalized to any Riemannian manifold including non-positive signatures by Greene [73] with independent orthogonal perturbations. It guarantees that the embedded geometry remains smooth (differentiable) after perturbations. With all these concepts, let us consider a Riemannian manifold V_4 with a non-perturbed metric $\bar{g}_{\mu\nu}$ being locally and isometrically embedded in a n-dimensional Riemannian manifold V_n given by a differentiable and regular map $\mathcal{X} : V_4 \to V_n$ satisfying the embedding equations

$$\mathcal{X}^A_{,\mu}\mathcal{X}^B_{,\nu}\mathcal{G}_{AB} = \bar{g}_{\mu\nu} \,, \quad (3)$$

$$\mathcal{X}^A_{,\mu}\bar{\eta}^B_a\mathcal{G}_{AB} = 0 \,, \quad (4)$$

$$\bar{\eta}^A_a\bar{\eta}^B_b\mathcal{G}_{AB} = \bar{g}_{ab} \,, \quad (5)$$

where we have denoted by $\mathcal{G}_{AB}$ the metric components of V_n in arbitrary coordinates, $\bar{\eta}$ denotes a non-perturbed unit vector field orthogonal to V_4. Concerning notation, capital Latin indices run from 1 to n. Small case Latin indices refer to the only one extra dimension considered. All Greek indices refer to the embedded space-time counting from 1 to 4. These set of equations represent the isometry condition Eq.(3), orthogonality between the embedding coordinates $\mathcal{X}$ and $\bar{\eta}$ in Eq.(4), and also, the vector normalization $\bar{\eta}$ and $\bar{g}_{ab} = \epsilon_a\delta_{ab}$ with $\epsilon_a = \pm 1$ in which the signs represent the signatures of the extra-dimensions. Hence, the integration of the system of equations Eqs.(3), (4) and (5) assures the configuration of the embedding map $\mathcal{X}$.

The second fundamental form, or more commonly, the non-perturbed extrinsic curvature $\bar{k}_{\mu\nu}$ of V_4 is by definition the projection of the variation of $\bar{\eta}$ onto the tangent plane :

$$\bar{k}_{\mu\nu} = -\mathcal{X}^A_{,\mu}\bar{\eta}^B_{,\nu}\mathcal{G}_{AB} = \mathcal{X}^A_{,\mu\nu}\bar{\eta}^B\mathcal{G}_{AB} \,, \quad (6)$$

where the comma denotes the ordinary derivative.

To obtain the embedded four-dimensional equations, one can take Eq.(2) written in the Gaussian frame embedding veilbein $\{\mathcal{X}^A_\mu, \bar{\eta}^A_a\}$. This reference frame is composed by a regular and differentiable coordinate $\{\mathcal{X}^A_\mu\}$ and a unitary normal vector $\{\bar{\eta}^A_a\}$. Accordingly, they define the basis of the embedded geometry and one can obtain the embedded four-dimensional field equations for

the background

$$R_{\mu\nu} - \frac{1}{2}Rg_{\mu\nu} + Q_{\mu\nu} = 8\pi G T_{\mu\nu} \,, \tag{7}$$

$$k^{\rho}_{\mu;\rho} - h_{,\mu} = 0 \,, \tag{8}$$

where in the trace of Codazzi equations in Eq.(8) we denote the mean Gaussian curvature by $h = g^{\mu\nu}k_{\mu\nu}$ and $h^2 = h.h$. The semi-colon denotes the ordinary covariant derivative.

The related cosmological model is obtained when considering the Friedman-Lemaître-Robertson-Walker (FLRW) metric in coordinates (r, θ, ϕ, t) as

$$ds^2 = \; dt^2 - a^2\left[dr^2 + f_\kappa^2(r)\left(d\theta^2 + \sin^2\theta d\varphi^2\right)\right] \,, \tag{9}$$

where $a = a(t)$ is the scale expansion factor, $f(r)_\kappa = \sin r$, r,$\sinh r$ and κ corresponds to spatial curvature $(1, 0, -1)$, respectively. For the present application, we consider a flat universe with $\kappa = 0$.

The $T_{\mu\nu}$ tensor is the four-dimensional energy-momentum tensor of a perfect fluid, expressed in co-moving coordinates as

$$T_{\mu\nu} = (p + \rho)U_\mu U_\nu + p\, g_{\mu\nu}, \quad U_\mu = \delta^4_\mu \,, \tag{10}$$

where U_μ is the co-moving four-velocity. The related conservation equation is given by

$$\rho + 3H\left(\rho + p\right) = 0 \,, \tag{11}$$

where ρ and p denote non-perturbed matter density and pressure, respectively.

Differently what happens to the usual General Relativity (GR) framework, the embedding between space-times leads to the appearance of the extrinsic terms. The deformation tensor $Q_{\mu\nu}$ is a geometrical term given by

$$Q_{\mu\nu} = g^{\rho\sigma}k_{\mu\rho}k_{\nu\sigma} - k_{\mu\nu}H - \frac{1}{2}\left(K^2 - h^2\right)g_{\mu\nu} \,, \tag{12}$$

where the term $K^2 = k^{\mu\nu}k_{\mu\nu}$ is the Gaussian curvature. It follows that $Q_{\mu\nu}$ is conserved in the sense of Noether's theorem

$$Q^{\mu\nu}{}_{;\nu} = 0 \,. \tag{13}$$

Using spatially flat Friedman-Lemaître-Robertson-Walker (FLRW) metric in Eq.(9), one obtains a solution of Eq.(8) that is given by

$$k_{ij} = \frac{b}{a^2}g_{ij}, \;\; i,j = 1,2,3, \quad k_{44} = \frac{-1}{\dot{a}}\frac{d}{dt}\frac{b}{a},$$

where $a \equiv a(t)$ is the usual expansion parameter and $b(t) \equiv b = k_{11}$ is the bending function that is function of time. The dot symbol denotes the ordinary time derivative.

Denoting the usual Hubble parameter by $H \equiv H(t) = \dot{a}/a$ and the extrinsic parameter $B \equiv B(t) = \dot{b}/b$, one obtains the following quantities by direct calculation of Eqs.(7) and (8)

$$k_{44} = -\frac{b}{a^2}(\frac{B}{H} - 1), \tag{14}$$

$$K^2 = \frac{b^2}{a^4}\left(\frac{B^2}{H^2} - 2\frac{B}{H} + 4\right), \quad h = \frac{b}{a^2}\left(\frac{B}{H} + 2\right), \tag{15}$$

$$Q_{ij} = \frac{b^2}{a^4}\left(2\frac{B}{H} - 1\right)g_{ij}, \; Q_{44} = -\frac{3b^2}{a^4}, \tag{16}$$

$$Q = -(K^2 - h^2) = \frac{6b^2}{a^4}\frac{B}{H} \,, \tag{17}$$

where in Eq.(16), we have denoted $i, j = 1..3$, with no sum on indices. Moreover, as shown in Refs.[20, 74], the dynamics of extrinsic curvature is formally completed in five-dimension by the analysis of the spin of a linear massless spin-2 fields in Minkowski space-time. As a consequence, it allow us in the cosmological context to find uniquely the bending function $b(t)$ starting from the Einstein-Gupta equations given by

$$\mathcal{F}_{\mu\nu} = 0 \,, \tag{18}$$

where they are defined as a copy (concerning its structure) of the usual Riemannian geometry. Hence, once can define a "f-Riemann tensor"

$$\mathcal{F}_{\nu\alpha\lambda\mu} = \; \partial_\alpha \Upsilon_{\mu\lambda\nu} - \; \partial_\lambda \Upsilon_{\mu\alpha\nu} + \Upsilon_{\alpha\sigma\mu}\Upsilon^{\sigma}_{\lambda\nu} - \Upsilon_{\lambda\sigma\mu}\Upsilon^{\sigma}_{\alpha\nu} \,,$$

$$\Upsilon_{\mu\nu\sigma} = \; \frac{1}{2}\left(\partial_\mu f_{\sigma\nu} + \partial_\nu f_{\sigma\mu} - \partial_\sigma f_{\mu\nu}\right) \,,$$

$$\Upsilon_{\mu\nu}{}^{\lambda} = f^{\lambda\sigma}\, \Upsilon_{\mu\nu\sigma}.$$

that were constructed from a "connection" associated with $k_{\mu\nu}$ and

$$f_{\mu\nu} = \frac{2}{K}k_{\mu\nu}, \;\; \text{and} \;\; f^{\mu\nu} = \frac{2}{K}k^{\mu\nu} \,, \tag{19}$$

in such a way that the normalization condition $f^{\mu\rho}f_{\rho\nu} = \delta^\mu_\nu$ applies. Thus, taking flat Friedman metric in Eq.(18), and with the results from Eqs.(7), (8) and (13) (by means of calculating $Q^\mu_{\mu,i} = 0$), one obtains the Friedman equation modified by the extrinsic curvature as

$$\left(\frac{\dot{a}}{a}\right)^2 = \frac{8}{3}\pi G\rho + \alpha_0 a^{2\beta_0 - 4}e^{\gamma^{\pm}(t)} \,, \tag{20}$$

where α_0 denotes an integration constant. As previously stated, with the aid of Gupta equations and the conservation of the deformation tensor, we can solve the homogeneity problem of Codazzi equations in Eq.(8) and we are able to define univocally the value of the k_{11} component of the extrinsic curvature, denoted by the bending function $b(t)$. Moreover, concerning the total energy density ρ, we denote $\rho = \rho_{mat} + \rho_{rad}$, which are the matter and radiation energy densities. The γ-exponent in the exponential function in Eq.(20) is defined as $\gamma^{\pm}(t) = \pm\sqrt{|4\eta_0 a^4 - 3|} \mp \sqrt{3}\arctan\left(\frac{\sqrt{3}}{3}\sqrt{|4\eta_0 a^4 - 3|}\right)$ that can be written in terms of redshift by means of the standard

relation $a = \frac{1}{1+z}$.

Based on previous cosmography tests [20, 22–24, 26], the parameter β_0 measures the magnitude of the deceleration parameter $q(z)$ and the values of parameter η_0 control the width of the transition phase redshift z_d from a decelerating to accelerating regime. In the aforementioned works, it was found that η_0 has a very small value $\eta_0 \to 0$ that leads to a transition redshift constraint $z_t < 1$ in compliance with observations. Hence, the related model is defined by Hubble evolution $H(z)$ as

$$H(z) = H_0\sqrt{\Omega_m(z) + \Omega_{rad}(z) + \Omega_{ext}(z)e^{\pm\gamma(z)}} \ , \quad (21)$$

where $H(z)$ is the Hubble parameter in terms of redshift z and H_0 is the current value of the Hubble constant. The matter density parameter is denoted by $\Omega_m(z) = \Omega_{m0}(1+z)^3$. The radiation density is given by $\Omega_{rad}(z) = \Omega_{rad0}(1+z)^4$ with $\Omega_{rad0} = \Omega_{m0}z_{eq}$ and the term $\Omega_{ext}(z) = \Omega_{ext0}(1+z)^{4-2\beta_0}\gamma_0$ stands for the density parameter associated with the extrinsic curvature. The integration constants were merged in the term γ_0. Concerning notation, the upper script "0" indicates the present value of any quantity. The equivalence number for the expansion factor a_{eq} given by

$$a_{eq} = \frac{1}{1+z_{eq}} = \frac{1}{(1 + 2.5\times10^4\Omega_{m0}h^2(T_{cmb}/2.7)^{-4})} \ , \quad (22)$$

where z_{eq} is the equivalence redshift. The CMB temperature is adopted for the value $T_{cmb} = 2.7255K$ and the Hubble factor $h = 0.67$. The complete form for Hubble parameter as in Eq.(21) at background level has been previously investigated in a series of studies [20, 22–24, 26].

In this work, we are based on the fact that competitive models must comply mild deviations of ΛCDM to reproduce its results, to correct its difficulties and to expand the theoretical landscape. In a search of such soft-after intents, we start dealing with cosmological perturbations with an approximation of Eq.(21) in high asymptotic redshift $z \to \infty$, or equivalently in terms of the asymptotic expansion factor around $a \sim 0$. At linear approximation, $\lim_{z\to\infty} e^{\gamma(z)} \sim 1 + \mathcal{O}(\gamma)$ it leads directly to a nearly resemblance with wCDM model with $H(z) \sim H_{wCDM}(z)$ at background level. At the moment, this allows us to obtain a more stable solutions. In these terms, the η_0 parameter vanishes accordingly. The current extrinsic contribution Ω^0_{ext} is given by the normalization condition for redshift at $z = 0$ that results in

$$\Omega^0_{ext} = \left(1 - \Omega^0_m - \Omega^0_{rad}\right) \ . \quad (23)$$

Hence, we can write the dimensionless Hubble parameter $E(z)$ as

$$E^2(z) = \Omega_{m0}(1+z)^3 + \Omega_{rad0}(1+z)^4 + \left(1 - \Omega_{m0} - \Omega_{rad0}\right)(1+z)^{4-2\beta_0} \ . \quad (24)$$

Hereon, the present model is denoted as β-model to facilitate the referencing.

III. MATTER EVOLUTION EQUATIONS IN CONFORMAL NEWTONIAN GAUGE

In longitudinal conformal Newtonian gauge, the metric in Eq.(9) is given by

$$ds^2 = a^2[(1+2\Phi)d\eta^2 - ((1-2\Psi)\delta_{ij}dx^i dx^j] \ , \quad (25)$$

where $\Phi = \Phi(\vec{x},\eta)$ and $\Psi = \Psi(\vec{x},\eta)$ denotes the Newtonian potential and the Newtonian curvature, respectively. The conformal time η is related with physical time as $dt = a(\eta)d\eta$.

The perturbed field equations of Eqs.(7) and (8) can be written as

$$\delta G^\mu_\nu = 8\pi G\delta T^\mu_\nu - \delta Q^\mu_\nu \ , \quad (26)$$

$$\delta k_{\mu\nu;\rho} = \delta k_{\mu\rho;\nu} \ . \quad (27)$$

Concerning notation, hereon the background quantities are represented by the tilde symbol.

To obtain the explicit form for perturbed field equations in Eqs.(26) and (27), we need to determine both perturbed metric $\delta g_{\mu\nu}$ and perturbed extrinsic curvature $\delta k_{\mu\nu}$. Using the main result of the Nash-Green theorem [72, 73], one can use the relation

$$\delta g_{\mu\nu} = -2\tilde{k}_{\mu\nu}\delta y \ , \quad (28)$$

where δy denotes an infinitesimal displacement of the extra dimension y in the bulk space and it is not considered in the line elements as in the case of rigid embedding models [11, 12].

The linear perturbations of a new geometry $\bar{g}_{\mu\nu}$ is given by $\bar{g}_{\mu\nu} = \tilde{g}_{\mu\nu} + \delta g_{\mu\nu}$ that can be written as

$$\bar{g}_{\mu\nu} = \tilde{g}_{\mu\nu} - 2\delta y\tilde{k}_{\mu\nu} \ , \quad (29)$$

and the related perturbed extrinsic curvature

$$\bar{k}_{\mu\nu} = \tilde{k}_{\mu\nu} - 2\delta y\ \tilde{g}^{\sigma\rho}\tilde{k}_{\mu\sigma}\tilde{k}_{\nu\rho} \ , \quad (30)$$

where we can identify $\delta k_{\mu\nu} = \tilde{g}^{\sigma\rho}\tilde{k}_{\mu\sigma}\tilde{k}_{\nu\rho}$. Using the Nash relation $\delta g_{\mu\nu} = -2\tilde{k}_{\mu\nu}\delta y$, we obtain

$$\delta k_{\mu\nu} = \tilde{g}^{\sigma\rho}\tilde{k}_{\mu\sigma}\delta g_{\nu\rho} \ . \quad (31)$$

The perturbation of the deformation tensor $Q_{\mu\nu}$ can be made from its background form in Eq.(12) and the resulting $k_{\mu\nu}$ perturbations from Nash's fluctuations in Eq.(31). Thus, one obtains

$$\delta Q_{\mu\nu} = -\frac{3}{2}(K^2 - h^2)\delta g_{\mu\nu} \ . \quad (32)$$

It is worthy noting that due to the Nash fluctuations in Eq.(29), we notice that Codazzi equations in Eq.(27) and the Einstein-Gupta equations in Eq.(18) are invariant un-

der perturbations and are confined to the background. Then using the background relations in Eqs.(14), (15), (16), and (17), we can determine the components of $\delta Q_{\mu\nu}$

$$\delta Q^i_j = \gamma_0 a^{2\beta_0-2}\Psi\delta^i_j \,, \tag{33}$$
$$\delta Q^i_4 = 0 \,, \tag{34}$$
$$\delta Q^4_4 = \gamma_0 a^{2\beta_0-2}\Phi\delta^4_4 \,, \tag{35}$$

where γ_0 is an integration constant that carries an extrinsic curvature term from the bending function $b(t)$ as seen in Eq.(20).

For a perturbed fluid with pressure p and density ρ, one can write the perturbed components of the related stress-tensor

$$\delta T^4_4 = \delta\rho \,, \tag{36}$$
$$\delta T^4_i = \frac{1}{a}(\rho_0 + p_0)\delta u_{\parallel i} \,, \tag{37}$$
$$\delta T^i_j = -\delta p\ \delta^i_j \,, \tag{38}$$

where $\delta u_{\parallel i}$ denotes the tangent velocity potential and ρ_0 and p_0 denote the non-perturbed components of density and pressure, respectively.

Moreover, we adopt the simplest condition for perturbations $\Psi = \Phi$ and obtain the following set of equations in the wave-number k-space of Fourier modes as

$$k^2\Phi_k + 3\mathcal{H}\left(\Phi_k^{'} + \Phi_k\mathcal{H}\right) = -4\pi G a^2\delta\rho_k + 9\gamma_0 a^{2\beta_0}\Phi_k \,, \tag{39}$$

$$(a\Phi_k)' = -4\pi G a^2(\rho_0 + p_0)\theta \,, \tag{40}$$

$$\Phi_k^{''} + 3\mathcal{H}\Phi_k' + (\mathcal{H}^2 + 2\mathcal{H}')\Phi_k - 9\gamma_0 a^{2\beta_0}\Phi_k = 4\pi G a^2(c_s^2\delta\rho_k) \,, \tag{41}$$

where $\mathcal{H} \equiv aH$ and $\theta = ik^j\delta u_{\parallel j}$ denotes the divergence of fluid velocity in k-space. We also use the relation $\delta p_k = c_s^2\delta\rho_k$ in which c_s denotes the sound speed. Hence, combining the aforementioned equations, we obtain the gravitational potential formula in k-space:

$$\Phi_k^{''} + 3(1+c_s^2)\mathcal{H}\Phi_k' + \left[k^2c_s^2 + (1+3c_s^2)\mathcal{H}^2 + 2\mathcal{H}'\right]\Phi_k = \gamma_0 a^{2\beta_0}(1+c_s^2)\Phi_k \,. \tag{42}$$

It is important to notice that when $\gamma_0 \to 0$ in Eq.(42), the standard GR correspondence is obtained. Thus, one recovers the subhorizon approximation with $k^2 >> \mathcal{H}^2$ or $k^2 >> a^2H^2$. Thus, Eq.(42) turns the Newtonian formula $\Phi_k \sim \frac{\delta\rho_k}{k^2}$.

After a Fourier transform, we perform the definition of the "contrast" matter density $\delta_m \equiv \frac{\delta\rho}{\rho_0}$. For a pressureless matter and a null anisotropic matter stress, we use Eq.(39) and obtain a relation of Φ_k and δ_m given by

$$k^2\Phi_k = -4\pi G_{eff}a^2\rho_0\delta_m \,, \tag{43}$$

where G_{eff} is the effective Newtonian constant and is given by

$$G_{eff}(a,k) = \frac{G}{1 - \frac{\gamma_0}{k^2}a^{2\beta_0}} \,, \tag{44}$$

where G is the Newtonian gravitational constant.

The corresponding equation of evolution of the contrast matter density $\delta_m(\eta)$ in conformal longitudinal Newtonian frame can be written as

$$\delta_m'' + \mathcal{H}\delta_m' - 4\pi G_{eff}a^2\rho_0\delta_m = 0 \,, \tag{45}$$

where the prime symbols denote derivatives with respect to conformal time η. And, in terms of the expansion factor $a(t)$, we obtain the contrast matter density $\delta_m(a)$ as

$$\ddot{\delta}_m(a) + \left(\frac{3}{a} + \frac{\dot{H}(a)}{H(a)}\right)\dot{\delta}_m(a) - \frac{3\Omega_{m0}G_{eff}/G}{2(H^2(a)/H_0^2)}\delta_m(a) = 0, \tag{46}$$

where the dot symbols denote derivatives with respect to scale factor a. As a matter of comparison, for GR $G_{eff} = G$ with the fluid parameter w and one obtains the solution

$$\delta(a) = a.2F_1\left(-\frac{1}{3w}, \frac{1}{2} - \frac{1}{2w}; 1 - \frac{5}{6w}; a^{-3w}(1-\Omega_m^{-1})\right) \,, \tag{47}$$

where $2F_1(a,b;c;z)$ is a hypergeometric function.

IV. OBSERVATIONAL CONSTRAINTS: ANALYSIS AND RESULTS

A. Statistical considerations on the data

In the following, we point out the main equations and statistical tools for the observational data on Growth fluctuations, CMB, BAO and the Pantheon SNIa. A complete set and description of these formulas can be found in details in Refs.[28–30, 61, 75].

1. *Growth fluctuations*

We use the σ_8 parameter that measures the growth of r.m.s fluctuations on the scale of $8h^{-1}$Mpc. This is performed by the measure of the quantity

$$f\sigma_8(a) \equiv f(a).\sigma_8(a) \,, \tag{48}$$

where $f(a) = \frac{\ln\delta}{\ln a}$ is the growth rate and the growth factor $\delta(a)$ is given by Eq.(46). To compatibilize the data dependence from the fiducial cosmology and another cosmological survey, it is necessary to rescale the growth-rate data by the ratio $r(z)$ of the Hubble parameter $H(z)$

and the angular distance $d_A(z)$ by using the relation

$$r(z) = \frac{H(z)d_A(z)}{H_f(z)D_f A(z)} \,, \tag{49}$$

where the subscript "f" corresponds a quantity of fiducial cosmology. Accordingly, the angular distance $d_A(z)$ is defined as

$$d_A(z) = \frac{c}{(1+z)}\int_z^0 \frac{1}{H(z')}dz' \,. \tag{50}$$

Likewise, the regulation of the χ^2 statistics is also necessary that relies on the definition

$$\chi^2(\Omega_{m0}, w, \sigma_8) = V^i C_{ij}^{-1} V_j \,, \tag{51}$$

where $V^i \equiv f\sigma_{8,i} - r(z_i)f\sigma_8(z_i, \Omega_{m0}, w, \sigma_8)$ denotes a set of vectors that goes up to ith-datapoints at redshift z_i for each $i = 1...N$ number of datapoints of a related collection of data. The set of $f\sigma_{8,i}$ datapoints come from theoretical predictions [28]. The set of C_{ij}^{-1} denotes the inverse covariance matrix. A final important correction concerns the necessity to disentangle the datapoints related to WiggleZ dark energy survey which, at first, are correlated. Then, the covariant matrix C_{ij} [48] is given by

$$C_{ij}^{wigglez} = 10^{-3}\begin{bmatrix} 6.400 & 2.570 & 0.000 \\ 2.570 & 3.969 & 2.540 \\ 0.000 & 2.540 & 5.184 \end{bmatrix} \tag{52}$$

and the resulting total matrix C_{ij}^{tot}

$$C_{ij}^{tot} = 10^{-3}\begin{bmatrix} \sigma_1^2 & 0 & 0 & ... \\ 0 & C_{ij}^{wigglez} & 0 & ... \\ 0 & 0 & ... & \sigma_N^2 \end{bmatrix} \tag{53}$$

where the set of σ^2's denote the N-variances.

2. CMB Planck2018 data

For the CMB data, we used the Planck2018 released [9] with χ^2-statistics

$$\chi^2_{CMB} = X^T_{Planck2018} C^{-1}_{CMB} X_{Planck2018} \,, \tag{54}$$

where the covariant matrix for the parameters for $R, l_A, \Omega_{b0}h^2$ is given by

$$X_{Plankc2018} = \begin{pmatrix} R - 1.7502 \\ l_A - 301.471 \\ \omega_b - 0.02236 \end{pmatrix} \tag{55}$$

where $\omega_b = \Omega_{b0}h^2$. The two shift parameters R and l_A are defined as the scale distance and acoustic scale, respectively, as

$$R = \frac{\sqrt{\Omega_{m0}}}{c} d_A(z_{CMB})(1+z_{CMB}) \,, \tag{56}$$

$$l_A = \frac{\pi d_A(z_{CMB})(1+z_{CMB})}{r_s(z_{CMB})} \,, \tag{57}$$

where the angular distance d_A is given by Eq.(50) and the related redshift at recombination z_{cmb} is given by

$$z_{CMB} = 1048[1+0.00124(\Omega_b h^2)^{-0.738}][1+g_1(\Omega_{m0}h^2)^{g_2}] \,, \tag{58}$$

and the parameters (g_1, g_2) are defined accordingly as

$$g_1 = \frac{0.0783(\Omega_b h^2)^{-0.238}}{1+39.5(\Omega_b h^2)^{0.763}} \,,\; g_2 = \frac{0.560}{1+21.1(\Omega_b h^2)^{1.81}} \,. \tag{59}$$

The comoving sound horizon $r_s(z)$ is given by

$$r_s(z) = c\int_z^\infty \frac{c_s(z')}{H(z')}dz' \,, \tag{60}$$

and the related sound speed c_s

$$c_s(z) = \frac{1}{\sqrt{3(1+\bar{R}_b/(1+z))}} \,, \tag{61}$$

with $\bar{R}_b = 31500\Omega_{b0}h^2(T_{CMB}/2.7K)^{-4}$. Moreover, the inverse of the covariant matrix C^{-1}_{CMB} for the parameters for $l_a, R, \Omega_{b0}h^2$ is given by $C^{-1}_{CMB} = \sigma_i\sigma_j C$, with $\sigma_i = (0.0046,\ 0.090,\ 0.00015)$ for the normalized covariance matrix given by

$$C = \begin{pmatrix} 1.00 & 0.46 & -0.66 \\ 0.46 & 1.00 & -0.37 \\ -0.66 & -0.33 & 1.00 \end{pmatrix} \tag{62}$$

3. BAO joint data

In a similar manner, we summarize some the useful formulas to work with BAO from the set of probes on SDSS [38–40], 6dFGS [41], IRAS [42, 43], 2MASS [42, 44], 2dFGRS [45], GAMA [46], BOSS[47], WiggleZ [48], Vipers [49], FastSound [50], BOSS Q [51] and additional points from the 2018 SSSD-IV [52–54].

We use the χ^2 statistics for WiggleZ in a form

$$\chi^2_{WiggleZ} = (\bar{A}_{obs} - \bar{A}_{th})C^{-1}_{WiggleZ}(\bar{A}_{obs} - \bar{A}_{th})^T \,, \tag{63}$$

where we denote the set of observational value $\bar{A}_{obs} = (0.447, 0.442, 0.424)$ for data vectors at $z = (0.44, 0.60, 0.73)$ compared with the theoretical predictions $\bar{A}_{th} = (z, p_i)$ is defined as

$$\bar{A}_{th} = d_V(z)\frac{\sqrt{\Omega_{m0}H_0^2}}{cz} \,, \tag{64}$$

with the dilation scale

$$d_V(z) = \frac{1}{H_0}\Big[(1+z)^2 d_A(z)^2 \frac{cz}{E(z)}\Big]^{1/3} . \quad (65)$$

Moreover, the inverse of the covariant matrix $C^{-1}_{WiggleZ}$ is given by

$$C^{-1}_{WiggleZ} = \begin{pmatrix} 1040.3 & -807.5 & 336.8 \\ -807.5 & 3720.3 & -1551.9 \\ 336.8 & -1551.9 & 2914.9 \end{pmatrix} . \quad (66)$$

Likewise, we adopt the same analysis on SDSS data such as

$$\chi^2_{SDSS} = (\bar{d}_{obs} - \bar{d}_{th}) C^{-1}_{SDSS} (\bar{d}_{obs} - \bar{d}_{th})^T , \quad (67)$$

from the comparison with the observable and theoretical distances d_{obs} and d_{th}, respectively. The distance $d_{obs} = (0.1905, 0.1097)$ is calculated at $z = 0.2$ and $z = 0.35$, and d_{th} is given by the definition

$$\bar{d}_{th} = \frac{r_s(z_d)}{d_V(z)} , \quad (68)$$

where the related comoving sound horizon $r_s(z)$ and sound speed $c_s(z)$ were given previously by Eqs.(60) and (61), respectively. In addition, the drag redshift is defined

$$z_{drag} = \frac{1291(\Omega_m h^2)^{0.251}}{1+0.659(\Omega_m h^2)^{0.828}}[1 + b_1(\Omega_m h^2)^{b_2}] , \quad (69)$$

where $b_1 = 0.313(\Omega_m h^2)^{-0.419}[1+0.607(\Omega_m h^2)^{0.674}]$ and $b_2 = 0.238(\Omega_m h^2)^{0.223}$.

The inverse of the covariant matrix C^{-1}_{SDSS} is given by

$$C^{-1}_{SDSS} = \begin{pmatrix} 30124 & -17227 \\ -17227 & 86977 \end{pmatrix} . \quad (70)$$

Finally, using the maximum likelihood, we combine all the data in

$$\chi^2_{BAO} = \chi^2_{WiggleZ} + \chi^2_{SDSS} + \chi^2_{6dF} + \chi^2_{SDSS-MGS} + \chi^2_{BOSS-LOWZ} + \chi_{BOSS-Ly_\alpha} . \quad (71)$$

4. The Pantheon supernova type Ia data

We determine the theoretical distance modulus $\mu_{th}(z)$ to obtain the constraints from SNIa and is given by

$$\mu_{th}(z) = 5\log_{10}(d_L(z)) + \mu_0, \quad (72)$$

where $\mu_0 = 42.38 - 5\log_{10}\mathbf{h}$ and $\mathbf{h} = 0.672$. The luminosity distance d_L related to Hubble expansion rate is given by

$$d_L(z|s,\mu_0) = (1+z)\int_0^z \frac{du}{E(u|s)} , \quad (73)$$

where s denotes the free parameters of a model. We use the prior for the density parameter of visible baryonic matter $\Omega_{b0} = 2.236/100\mathbf{h}^2$. The χ^2 statistics are used in a form

$$\chi^2_{SnIa}(s|\mu_0) = \sum_{i=1}^{n} \frac{[\mu_{th,i}(s,\mu_0|z_i) - \mu_{obs,i}(z_i)]}{\sigma^2_{\mu i}} , \quad (74)$$

where $n = 1048$ is the number of events of the Pantheon SNIa data [31], the distance modulus obtained from observations is denoted by $\mu_{obs,i}(z_i)$, and $\sigma_{\mu i}$ is the total uncertainty of the observational data.

B. Results and discussion

The methodology used in this paper relies on the Markov Chain Monte Carlo (MCMC) sample technique adapted from the publicly available code of a modified Metropolis–Hastings algorithm [29, 30] to infer the parameter likelihoods. We perform our analysis using the joint likelihood of kinematical probes on the CMB Planck 2018 data [9], the Pantheon SNIa [31] with redshift ranging from $0.01 < z < 2.3$, the Hubble parameter $H(z)$ as a function of redshift [32–37] and the "extended Gold 2018" compilation of the CMB Planck 2018 (TT, TE, EE+lowE) within the 68% intervals best-fit parameters using the data points of SDSS [38–40], 6dFGS [41], IRAS [42, 43], 2MASS [42, 44], 2dFGRS [45], GAMA [46], BOSS [47], WiggleZ [48], Vipers [49], FastSound [50], BOSS Q [51] and additional points from the 2018 SSSD-IV [52–54].

To apply our χ^2-statistics, we extract the data points from the Pantheon SNIa, CMB, BAO, Hubble parameter and growth, with the amount of 1048, 3, 9, 36 and 25 data points, respectively, with a total of 1121 data points. In order to keep the analysis on the sub-horizon linear scale, we set the minimum value of expansion parameter as $a_{min} = 0.001$ and $k = 300\ H_0 \sim 0.1\mathrm{hMpc}^{-1}$. Thus, we use the parameter vectors $\{\Omega_{m0}, 100\Omega_b h^2, h, \beta_0, \sigma_8\}$ with the adopted priors $\{(0.001, 1), (0.001, 0.08), (0.4, 1), (1.9, 2.001), (0.1, 1.8)\}$, respectively. To the CMB temperature, we adopt a reference value $T_{cmb} = 2.7255K$. Moreover, the joint analysis was also implemented by the product of the particular likelihoods $\mathcal{L}$ for each data set

$$\mathcal{L}_{tot} = \mathcal{L}_{Pantheon}.\mathcal{L}_{BAO}.\mathcal{L}_{CMB}.\mathcal{L}_{H(z)}.\mathcal{L}_{growth} \quad (75)$$

and the sum of individual χ^2 to get the total χ^2

$$\chi^2_{tot} = \chi^2_{Pantheon} + \chi^2_{BAO} + \chi^2_{CMB} + \chi^2_{H(z)} + \chi^2_{growth} . \quad (76)$$

The list of full values for the $H(z)$ data can be found in Table 1 and 2 in Ref.[30].

We compare our results with three phenomenological models to ascertain how the β-model is constrained to available data. In Table I and II, we present the best-fit

TABLE I. A summary of best-fit values of the background parameters calculated by using MCMC chains with the resulting χ^2 values. The χ^2_{bf} denotes the χ^2 best-fit values from MCMC and χ^2_{red} refers to reduced χ^2 from the value of the total χ^2 of minimizing all data and the related degree of freedom. For the sake of convenience, we refer the present model in this paper as β-model as shown below. Errors were obtained directly from the covariant matrix of the MCMC chain.

Model	Ω_{m0}	$100\Omega_{b0}h^2$	h	σ_8	Model parameters	χ^2_{red}	χ^2_{bf}
ΛCDM	0.317± 0.006	2.234± 0.015	0.674± 0.004	0.758± 0.028	$w=-1$	0.974	1087.82
wCDM	0.312± 0.008	2.233± 0.015	0.679± 0.008	0.760± 0.028	$w=-1.023\pm 0.033$	0.974	1087.40
CPL	0.309± 0.007	2.223± 0.015	0.688± 0.007	0.757± 0.028	$w=-0.939\pm 0.027$ $wa=-0.595\pm 0.090$	0.982	1095.15
β-model	0.316± 0.006	2.238± 0.015	0.674± 0.004	0.756± 0.028	β_0=1.992± 0.013	0.975	1088.16

TABLE II. A summary of mean values of background parameters calculated by using MCMC chains with the main parameters.

Model	Ω_{m0}	$100\Omega_{b0}h^2$	h	σ_8	Model parameters
ΛCDM	0.316± 0.006	2.235± 0.015	0.674± 0.004	0.761± 0.028	$w=-1$
wCDM	0.312± 0.007	2.234± 0.015	0.680± 0.008	0.759± 0.028	$w=-0.993\pm0.027$
CPL	0.301± 0.006	2.223± 0.015	0.699± 0.007	0.755± 0.029	w=-0.944± 0.028 wa=-0.795± 0.122
β-model	0.320± 0.006	2.238± 0.016	0.669± 0.005	0.761± 0.028	β_0=1.965± 0.014

and mean values for the studied models.

In Fig.(1), it is shown the results of $(\sigma_8 - \Omega_m)$ contours from the MCMC chains. From the right-to-left top panels show the results of the β-model and ΛCDM. From the bottom right-to-left panels show the results of the GR quintessence and CPL model, respectively. We also compare the values of σ_8 from Planck 2015 (red points) and Planck 2018 (blue points) with the mean values (black points) of the related models. For the β-model, it shows a close proximity with the ΛCDM results with a decrease of the σ_8 tension from 3-σ to 2-σ contours. A similar result is presented in the bottom left-panel with GR-quintessence. On the other hand, in the CPL-model (bottom right-panel) the σ_8 tension is aggravated. In addition, Fig.(2) shows the probability density function (PDF) of the cosmological parameters of the β-model. In particular, due to its several minima in the likelihood the obtained degeneracies in the values of the β-parameter show an interesting situation to decrease more the σ_8 tension to 1-σ contour, which is not possible to happen in the ΛCDM model.

In order to check the statistical relevance of the models as compared to observations, a reference can be made with using the AIC classifiers to estimate the tension between the data fitting and particular models. To sum up, they are used to infer how much information is lost when the *true* (unknown) model is replaced by a particular one. In this sense, the model with higher AIC tends to aggravate the tension which commonly happens when more parameters are allowed. To apply this criteria, we firstly adopt the errors from the data being as Gaussian and use AIC to evaluate the fit-to-data for small samples sizes [77, 78] by the formula

$$AIC = \chi^2_{bf} + 2k\frac{2k(k+1)}{N-k-1}\,, \tag{77}$$

where χ^2_{bf} is the best fit χ^2 of the model, k represents the number of the uncorrelated (free) parameters and N is the number of the data point in the adopted dataset. The difference $|\Delta AIC| = AIC_{model\ (2)} - AIC_{model\ (1)}$ represents the Jeffreys' scale [79] that measures the intensity of tension between two models. Higher values for $|\Delta AIC|$ denotes more tension between models and more statistically uncorrelated they are. For $|\Delta AIC \leq 2|$ the models are statistically consistent with a considerable level of empirical support. For $4 < \Delta AIC < 7$ indicates a positive tension against the model with a higher value of AIC. For $|\Delta AIC \geq 10|$ defines a strong evidence against the model with a higher AIC.

In Table III, it is shown the results of the classification of the AIC analysis showing a statistical equivalence between the ΛCDM and wCDM models and a nearly equivalence of these models with the β-model that has ΔAIC roughly close to 2. On the other hand, the CPL model is ruled out with a strong evidence against it.

As previously mentioned in the introduction section, we proceed further adopting a different direction in the analysis. We apply again the MCMC chains to our χ^2-statistics with no consideration of CMB nor BAO data, in order to realize the consequences on the evolution of kinematical parameters $H(z)$, $q(z)$ and the transition redshift z_t. This relies on the fact that the kinematical probes are model independent and we use the data on the Pantheon SNIa and $H(z)$ with some galaxy clustering [32–37] with the total amount of 1084 data points with a particular likelihoods $\mathcal{L}$ for each data set

$$\mathcal{L}_{tot} = \mathcal{L}_{Pantheon}.\mathcal{L}_{H(z)} \tag{78}$$

and the sum of individual χ^2 to get the total χ^2

$$\chi^2_{tot} = \chi^2_{Pantheon} + \chi^2_{H(z)}\,. \tag{79}$$

Due to the previous results of the AIC analysis in Table III, we do not consider the CPL model for this new

TABLE III. A summary of the obtained values of AIC for the studied models.

Model	AIC	ΔAIC	Evidence against the model
ΛCDM	1095.86	0	null
wCDM	1097.45	1.60	weak
CPL	1107.23	11.37	strong
β-model	1098.21	2.36	substantially weak

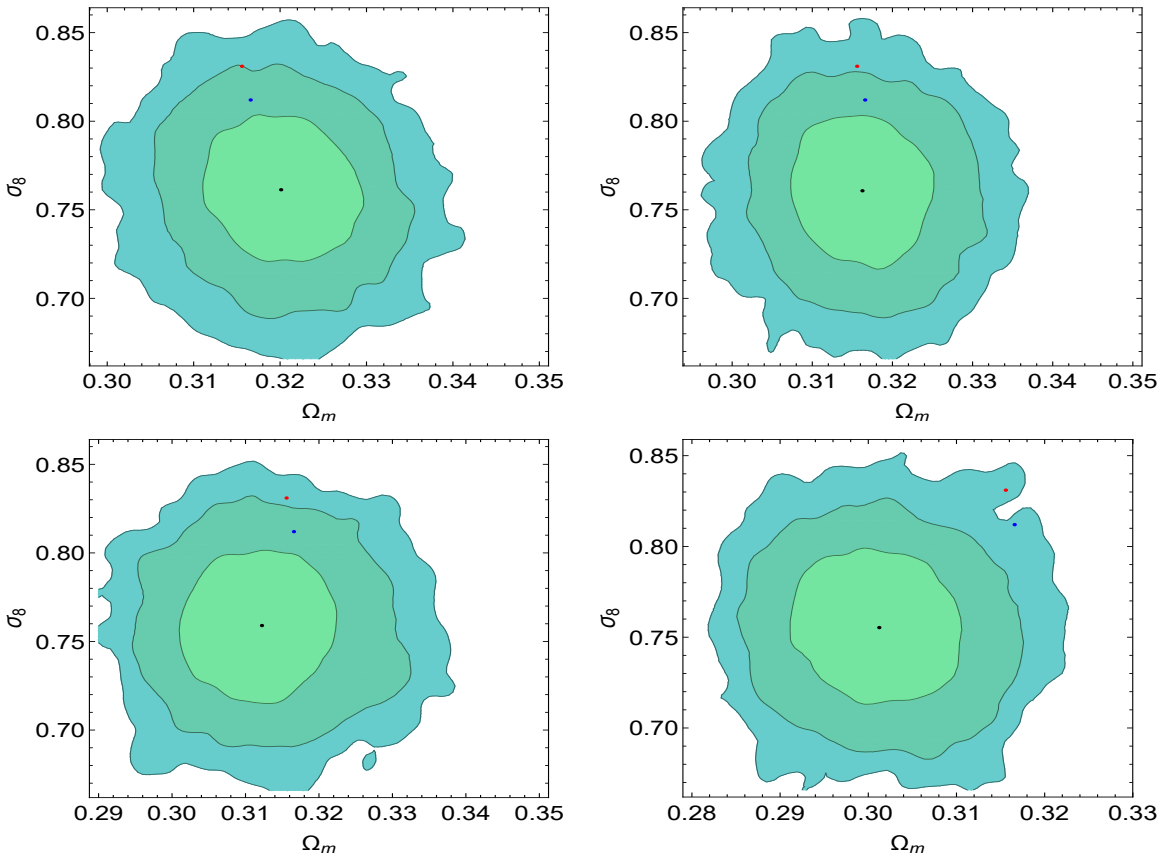

FIG. 1. Contour regions at 1-σ, 2-σ and 3-σ with 68.3%, 95.4% and 99.7% confidence levels, respectively, in the plane $(\sigma_8 - \Omega_m)$. Red points mark the CMB Planck 2015 data, whereas the blue points indicate CMB Planck 2018 data. Black points refer to the mean values of the parameters resulting from MCMC chains.

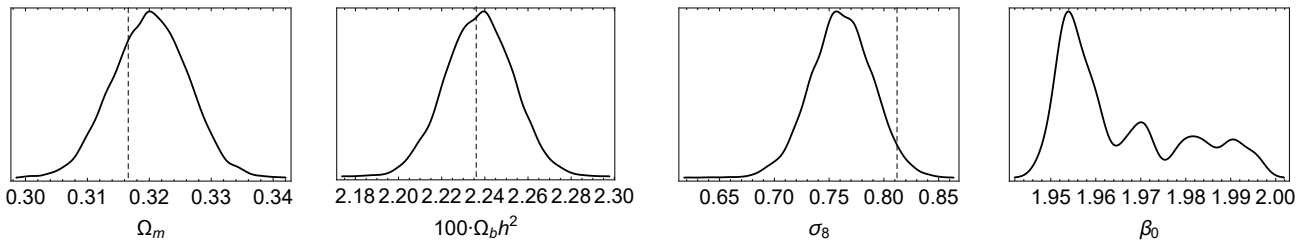

FIG. 2. One-dimensional PDF likelihood of the cosmological parameters for the cosmological parameters in the β-model used in this study. The vertical dashed lines indicate the CMB Planck 2018 values. In particular, the panel also shows the degeneracies for the β_0 values.

MCMC analysis. Accordingly, the results are shown in Tables IV and V. The results of the AIC analysis is presented in Table VI that reinforces the statistical compatibility between the models.

The transition redshift can be found from the deceler-

TABLE IV. A summary of best-fit values of the background parameters calculated by using MCMC chains with the resulting χ^2 values for the Pantheon SNIa and $H(z)$ data. The χ^2_{bf} denotes the χ^2 best-fit values from MCMC and χ^2_{red} refers to reduced χ^2 from the value of the minimum χ^2 and the related degree of freedom. For the sake of convenience, we refer the present model in this paper as β-model as shown below. Errors were obtained directly from the covariant matrix of the MCMC chain.

Model	Ω_{m0}	h	Model parameters	χ^2_{red}	χ^2_{bf}
ΛCDM	0.285± 0.016	0.685± 0.014	$w=-1$	0.978	1056.56
wCDM	0.263± 0.021	0.687± 0.016	$w=-0.918\pm 0.046$	0.978	1055.45
β-model	0.270± 0.018	0.687± 0.015	β_0=1.915± 0.014	0.978	1055.56

TABLE V. A summary of mean values of background parameters calculated by using MCMC chains with the main parameters.

Model	Ω_{m0}	h	Model parameters
ΛCDM	0.285± 0.016	0.684± 0.014	$w=-1$
wCDM	0.276± 0.021	0.685± 0.015	$w=-0.963\pm0.044$
β-model	0.276± 0.017	0.686± 0.017	β_0=1.952± 0.014

ation parameter in a form

$$q(z)=\frac{1}{H(z)}\frac{dH(z)}{dz}(1+z)-1\,. \tag{80}$$

Hence, we can write

$$q(z)=\frac{3}{2}\left[\frac{\Omega_{\,m}(z)+\Omega_{rad}(z)+\gamma^{*}\Omega_{\,ext}(z)}{\Omega_{\,m}(z)+\Omega_{rad}(z)+\Omega_{\,ext}(z)}\right]-1\;\;, \tag{81}$$

where $\gamma^{*}=\frac{1}{3}\left[4-2\beta_0\right]$.

We use the best-fit values of the cosmological parameters in Tables III and IV for the calculation of the resulting $H(z)$ and $q(z)$ from Eqs.(21) and (81). The behaviour of the transition redshift z_t in terms of the matter distribution Ω_m. Taking equation Eq.(81) and calculating the deceleration parameter $q(z)=0$ (neglecting the radiation contribution), we can find the transition redshift z_t as

$$z_t=\left(\frac{2(\beta_0-1)(1-\Omega_{m0})}{\Omega_{m0}}\right)^{\frac{1}{2\beta_0-1}}-1\,. \tag{82}$$

It it worth noting that the same formula of z_t for ΛCDM model is obtained for $\beta_0=2$. From the related MCMC chains, in Fig.(3) shows the one-dimensional PDF likelihood that presents several minima for the values of β_0 values of the β-model that allows more possibilities to compatibilize the current and future observations on the acceleration expansion. In Fig.(4) we show the evolution of the Hubble function $H(z)$ for the complete pack of data considering CMB, BAO, cosmic growth, the Pantheon SNIa and $H(z)$. In Fig.(5), it is shown the related evolution of the models for Pantheon SNIa+$H(z)$, and some clustering on $H(z)$. For both situations, the best-fit values for the parameters are shown in the panels. The differences of both figures are noted from $z>1$ where the effects of CMB and BAO are more pronounced. This can be noted in Fig.(4) that shows larger values on $H(z)$. On the other hand, Fig.(4) shows the curves that tend to a mild damping on the $H(z)$ values for late times. This

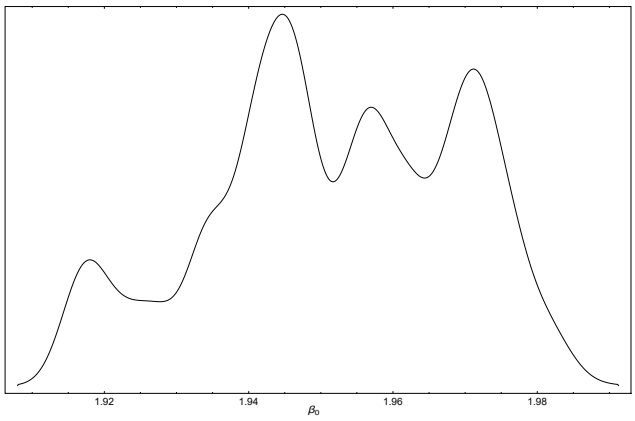

FIG. 3. One-dimensional PDF likelihood of that shows the degeneracies for the β_0 values.

difference may be originated in the mild tension between CMB Planck data and growth measurements at low redshift. This may be solved by the degeneracies of the β_0 values since the percentage relative difference is up to 3.87%.

In Figs.(6) and (7), it is shown the behavior of the deceleration parameter $q(z)$ as a function of redshift when considering the set of CMB, BAO, cosmic growth, the Pantheon SNIa and $H(z)$, and the other group as that of the Pantheon SNIa+$H(z)$, respectively. For both situations, we have an accelerated regime for late times and decelerating pattern for early times. The best-fit values for the parameters are shown in the panels. In Fig.(6) shows an overall transition of the models roughly at $z_t\sim 0.6$ with a related value of the deceleration parameter as measured today q_0 roughly at ~ -0.5.

The situation is changed when analysing Fig.(7) that indicates an earlier transition around $z_t\sim 0.7$. What concerns the value of q_0, it maintains the same pattern for β-model with $q_0=-0.533\pm0.027$ with a low percentage relative difference is up to 2.30% in comparison with the previous case. Due to the present degeneracies on the

TABLE VI. A summary of the obtained values of AIC for the studied models. We adopt ΛCDM as a reference.

Model	AIC	ΔAIC	Evidence against the model
ΛCDM	1064.60	0	null
wCDM	1065.51	0.91	weak
β-model	1065.62	1.02	weak

values of β parameter, the β-model is not sensitive to the variations of model dependent probes, as that of CMB and BAO data, with a percentage relative difference up to 3% that makes the possibility to gather feasible information for cosmokinetics analysis considering a larger pack of data, even the Pantheon SNIa and $H(z)$ data are model independent, apart from systematics eventually involved. This is also in accordance with independent fits in literature as in, e.g., with $z_t = 0.64^{+0.11}_{-0.07}$ [80], and BAO/CMB + SNIa constraints, with MLCS2K2 light-curve fitter $z_t = 0.56^{+0.13}_{-0.10}$ and with SALT2 fitter, $z_t = 0.64^{+0.13}_{-0.07}$ with 68% confidence level [81].

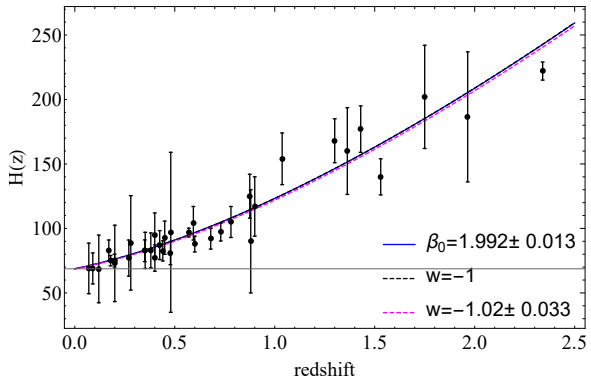

FIG. 4. Evolution of the Hubble parameter $H(z)$ as a function of redshift. The related best-fit values are show in the panel for the models with the full data on CMB, BAO, cosmic growth, the Pantheon SNIa and $H(z)$.

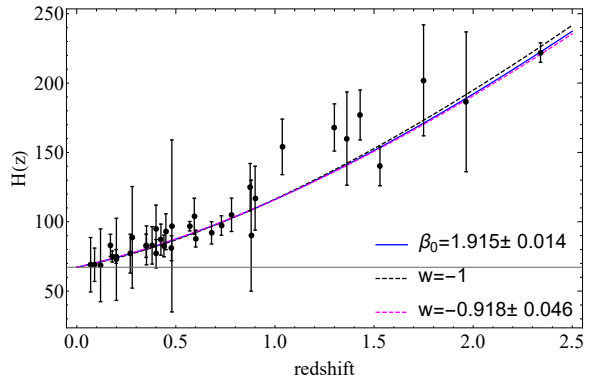

FIG. 5. Evolution of the Hubble parameter $H(z)$ as a function of redshift. The related best-fit values are show in the panel for the models with the data on the Pantheon SNIa+$H(z)$.

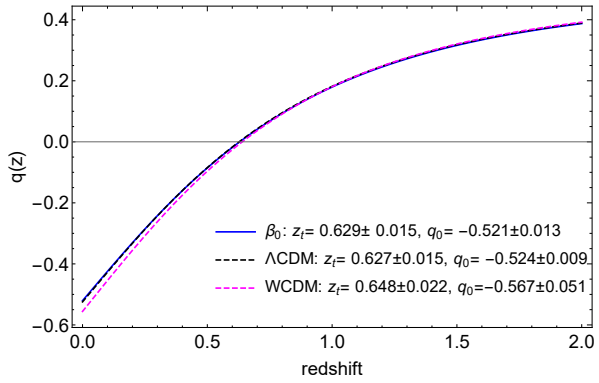

FIG. 6. Evolution of the deceleration parameter $q(z)$ as a function of redshift. The best-fit values of the transition redshift is also indicated. The related values are show in the panel for the models with the full data on CMB, BAO, cosmic growth, the Pantheon SNIa and $H(z)$.

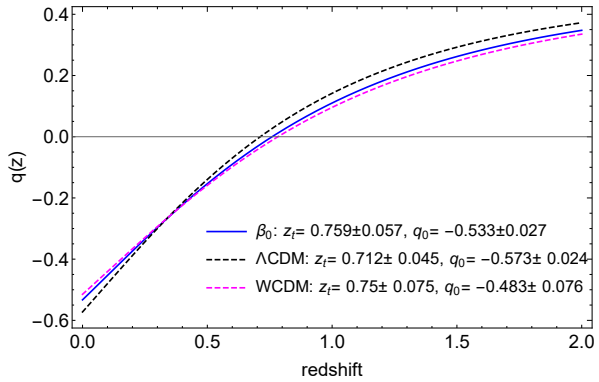

FIG. 7. Evolution of the deceleration parameter $q(z)$ as a function of redshift. The best-fit values of the transition redshift is also indicated. The related values are show in the panel for the models with the data on the Pantheon SNIa+$H(z)$.

V. REMARKS

In this paper, we discussed the dark energy problem with a proposal of a geometric model based on the Nash-Green embedding theorem. Using the corresponding modified Friedman equation in a flat background, we confronted the present model to popular models like ΛCDM, wCDM and CPL through a joint analysis on recent pack of datasets on the Pantheon SNIa, CMB, BAO, cosmic growth and the Hubble $H(z)$ evolution. We also proposed a comparison of the aforementioned pack with the model-independent data of the Pantheon SNIa+$H(z)$ to

the analysis on the cosmokinetics quantities, i.e., $H(z)$ and the deceleration parameter $q(z)$. The cosmography analysis on CMB and BAO observations is model dependent and may lead to higher statistical and/or systematic errors, but they can be attenuated by the joint analysis and/or improvement of the technical observational measurements through the years to come. For instance, BAO measurements involves the assumption of fiducial cosmology in the construction of the observables that lead to the necessity of rescaling and homogenizing the raw data. From the CMB part, the high signal-to-noise CMB map should be cleaned by both kinetics and thermal Sunyaev-Zel'dovich effects in clusters [82, 83]. These difficulties turn the jointly analysis an additional issue to cosmography and cosmological models must deal with such subtleties in a search of a complete description of the universe.

In this direction, we used a Markov Chain Monte Carlo analysis (MCMC) from a modified Metropolis–Hastings algorithm [29, 30] to determine the cosmic parameters. We found that in the studied models, except for CPL model, are nearly statistically equivalent at 1-σ confidence level with the ΔAIC values roughly around 2. The 3-σ tension of the CMB Planck 2015 and growth data was reduced to a mild 2-σ tension using the CMB Planck 2018 and may be reduced to 1-σ contour by the appearance of degeneracy values of the β-model consistent with the behaviour of $f\sigma_8$. When studying the cosmography parameters $H(z)$ and $q(z)$, we found that the inclusion of the CMB+BAO+Growth data gives larger values for $H(z)$ in early times and a later transition $z_t \sim 0.6$ as compared with the analysis using the Pantheon+$H(z)$ data alone. These differences cease to be in the context of the β-model since their degeneracies on the β-parameter allow to reduce the observed mild discrepancy of the curves in $H(z)$ from $z > 1$ as shown in Figs.(4) and (5). As an overall conclusion, this turns the β-model capable of analysing the cosmography parameters within a feasible range of confidence level with a more complete jointly data, apart from systematics. It reinforces the evidences for cosmic acceleration in a truly model-independent regardless of the nature of the probes. As future prospects, we intend to investigate the evolution of the background with the evaluation of the evolution equations of the perturbations in order to confront the behaviour of the viscosity parameter and growth index rate and signatures on the Integrated Sachs–Wolfe (ISW) effect. This process is in due course and will be reported elsewhere.

ACKNOWLEDGMENTS

A. J. S. Capistrano thanks Federal University of Latin-American Integration for financial support from Edital PRPPG 110 (17/09/2018) and Fundação Araucária/PR for the Grant CP15/2017-P&D 67/2019. P.T.Z. Seidel thanks the Coordination for the Improvement of Higher education Personnel (Capes-Brazil) for the scholarship grant. H. R. Duarte thanks Federal University of Latin-American Integration for the scholarship grant Bolsa DS/Unila.

[1] R. J. Nemiroff, R. Joshi, B.R. Atla, JCAP**06**, 006 (2015).
[2] B. Santos, A. A. Coley, N. Chandrachani Devi, J. S. Alcaniz, JCAP**02**, 047 (2017).
[3] P. Kumar, C.P. Singh, Astrophys Space Sci.**362**, 52 (2017).
[4] H.E.S. Velten, R.F. vom Marttens, W. Zimdahl, Eur. Phys. J. C**74**, 11, 3160 (2014).
[5] J. Sultana, Monthly Not. R. Astron. Soc. **457(1)**, 212-216 (2016).
[6] N. Sivanandam, Phys. Rev. D**87**, 083514 (2013).
[7] K. Nozari, N. Behrouz, N. Rashidi, Adv. High En. Phys., 569702, (2014).
[8] P. A. R. Ade et al. (Planck Collaboration), Astron. Astrophys.**594**, A13 (2016).
[9] N. Aghanim et al., (Planck Collaboration), Planck 2018 results. VI. Cosmological Parameters, ArXiv:1807.06209.
[10] N. Arkani-Hamed, S. Dimopoulos, G. Dvali, Phys. Lett., B**429**, 263 (1998).
[11] L. Randall, R. Sundrum, Phys. Rev. Lett.**83**, 3370 (1999).
[12] L. Randall, R. Sundrum, Phys. Rev. Lett.**83**, 4690 (1999).
[13] G. Dvali, G. Gabadadze, M. Porrati, Phys. Lett.B**485**, 208-214 (2000).
[14] R. A. Battye, B. Carter, Phys. Lett. B**509**, 331 (2001).
[15] M.D. Maia, E.M. Monte, Phys. Lett. A **297**, 9-19, (2002).
[16] M.D. Maia, E.M. Monte, J.M.F. Maia, J.S. Alcaniz, Class. Quantum Grav.**22**, 1623 (2005).
[17] M.D. Maia, N. Silva, M.C.B. Fernandes, JHEP**04**, 047 (2007).
[18] M. Heydari-Fard, H. R. Sepangi, Phys.Lett., B**649**, 1-11 (2007).
[19] S. Jalalzadeh, M. Mehrnia, H. R. Sepangi, Class. Quant. Grav.**26**,155007 (2009).
[20] M.D. Maia, A.J.S Capistrano, J.S. Alcaniz, E.M. Monte, Gen. Rel. Grav.**10**, 2685 (2011).
[21] A. Ranjbar, H.R. Sepangi, S. Shahidi, Ann. Phys.**327**, 3170-3181 (2012).
[22] A. J. S. Capistrano, L.A. Cabral, Ann. Phys. **384**, 64-83(2014).
[23] A. J. S. Capistrano, Monthly Not. Roy. Astron. Soc.**448**, 1232-1239 (2015).
[24] A. J. S. Capistrano, L. A. Cabral, Class. Quantum Grav. **33**, 245006 (2016).
[25] A. J. S. Capistrano, A. C. Gutiérrez-Pi˜ñeres, S. C. Ulhoa, R. G.G. Amorim, Ann. Phys.**380**, 106–120 (2017).
[26] A. J. S. Capistrano, Ann. Phys. (Berlin), 1700232 (2017).
[27] A.J. S. Capistrano, Phys. Rev. D **100**, 064049-1 (2019).
[28] S. Nesseris, G. Pantazis, L. Perivolaropoulos, Phys. Rev. D**96**, 2, 023542 (2017).

[29] C. A. Luna, S. Basilakos, S. Nesseris, Phys. Rev. D**98**, 023516 (2018).
[30] R. Arjona, W. Cardona, S. Nesseris, Phys. Rev. D**99**, 043516 (2019).
[31] D. M. Scolnic et al., Astrophys. J.**859**, 101 (2018).
[32] C. Zhang, H. Zhang, S. Yuan, T.J. Zhang, Y.-C. Sun, Res. Astron. Astrophys.**14**, 1221 (2014).
[33] D. Stern, R. Jimenez, L. Verde, M. Kamionkowski, S. A. Stanford, JCAP**1002**, 008 (2010).
[34] M. Moresco et al., JCAP**1208**, 006 (2012).
[35] C.H. Chuang, Y. Wang, Monthly Not. R. Astron. Soc.**435**, 255 (2013).
[36] M. Moresco, Monthly Not. R. Astron. Soc.**450**, L16 (2015).
[37] T. Delubac et al. (BOSS), Astron. Astrophys.**574**, A59 (2015).
[38] L. Samushia, W. J. Percival, A. Raccanelli, Monthly Not. R. Astron. Soc. **420**, 2102 (2012).
[39] C. Howlett, A. Ross, L. Samushia, W. Percival, M. Manera, Monthly Not. R. Astron. Soc. **449**, 1, 848 (2015).
[40] M. Feix, A. Nusser, E. Branchini, Phys. Rev. Lett. **115**, 1, 011301 (2015).
[41] D. Huterer, D. Shafer, D. Scolnic, F. Schmidt, JCAP**1705**, 05, 015 (2017).
[42] M. J. Hudson, S. J. Turnbull, Astrophys. J.**751**, L30 (2013).
[43] S. J. Turnbull, et al., Monthly Not. R. Astron. Soc. **420**, 447 (2012).
[44] M. Davis et al., Monthly Not. R. Astron. Soc. **413**, 2906 (2011).
[45] Y. S. Song, W. J. Percival, JCAP**0910**, 004 (2009).
[46] C. Blake et al., Monthly Not. R. Astron. Soc.**436**, 3089 (2013).
[47] A. G. Sanchez et al., Monthly Not. R. Astron. Soc. **440**, 3, 2692 (2014).
[48] C. Blake et al., Monthly Not. R. Astron. Soc.**425**, 405 (2012).
[49] A. Pezzotta et al., Astron. Astrophys.**604**, A33 (2017).
[50] T. Okumura et al., Publ. Astron. Soc. Jap.**68**, 3, 38 (2016).
[51] P. Zarrouk et al., Monthly Not. R. Astron. Soc.**477**, 2, 1639 (2018).
[52] Héctor Gil-Marín et al., Monthly Not. R. Astron. Soc.**477**, 2, 1604-1638 (2018).
[53] J. Hou et al., Monthly Not. R. Astron. Soc.**480**, 2, 2521-2534 (2018).
[54] Gong-Bo Zhao et al., Monthly Not. R. Astron. Soc.**482**, 3, 3497-3513 (2019).
[55] X. Fan, N. A. Bahcall, R. Cen., Astrophy. J. Lett. **490**, 123 (1997).
[56] O. Farooq, B. Ratra, Astrophys. Journ. Lett.**766**, 1 (2013).
[57] R. Lazkoz, J. Alcaniz, C. Escamilla-Rivera, V. Salzano, I. Sendra, JCAP**12**, 005 (2013).
[58] S. Capozziello, O. Luongo, E. N. Saridakis, Phys. Rev. D**91**, 124037 (2015).
[59] D. Muthukrishna, D. Parkinson, JCAP**11**, 052 (2016).
[60] M. Moresco, F. Marulli, Monthly Not. R. Astron. Soc. **471**, L82–L86 (2017).
[61] A. B. Rivera, J. E. García-Farieta, Intern. Journal Mod. Phys. D**28**, 9 , 1950118 (2019).
[62] N. Cruz, A. Hernández-Almada, O. Cornejo-Pérez, Phys. Rev. D**100**, 083524 (2019).
[63] C. A. P Bengaly, Monthly Not. R. Astron. Soc. Lett. slaa**040**, 2020.
[64] R.R. Caldwell, R. Dave, P.J. Steinhardt, Phys. Rev. Lett.**80**, 1582 (1998).
[65] B. Ratra, P. J. E. Peebles, Phys. Rev. D**37**, 3406 (1988).
[66] M. Chevallier, D. Polarski, Int. J. Mod. Phys. D**10**, 213 (2001).
[67] E. V. Linder, Phys. Rev. Lett.**90**, 091301 (2003).
[68] H. Akaike, IEEE Transact. Autom. Control **19**, 716 (1974).
[69] S. K. Donaldson, Contemporary Mathematics (AMS)**35**, 201 (1984).
[70] C. H. Taubes, Contemporary Mathematics (AMS)**35**, 493 (1984).
[71] C.S. Lim, Prog. Theor. Exp. Phys., 02A101 (2014).
[72] J. Nash, Ann. Maths.**63**, 20 (1956).
[73] R. Greene, Memoirs Amer. Math. Soc.**97**, (1970).
[74] S.N. Gupta, Phys. Rev.**96**, 6 (1954).
[75] D. J. Eisenstein, W. Hu, Astrophys. J. **496**, 605 (1998).
[76] M.S. Turner, M. White, Phys. Rev. D**56**, 4439 (1987).
[77] A. R. Liddle, Monthly Not. R. Astron. Soc.**377**, L74–L78 (2007).
[78] N. Sugiura, Commun. Stat. A, Theory Methods **7**, 13 (1978).
[79] H. Jeffreys, Theory of Probability, 3rd edn. Oxford Univ. Press, Oxford, (1961).
[80] M. Moresco et al., JCAP**12**, 039 (2016).
[81] R. Giostri *et al.*, JCAP**1203**, 027 (2012).
[82] W. Hu, D. E. Holz, C. Vale, Phys. Rev. D**76**, 127301 (2007).
[83] J. Yoo, M. Zaldarriaga, L. Hernquist, Phys. Rev. D**81**, 123006 (2010).